Molecular Catalysis 528 (2022) 112461

Contents lists available at ScienceDirect

Molecular Catalysis

journal homepage: www.journals.elsevier.com/molecular-catalysis

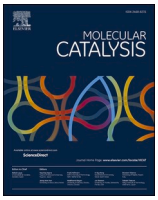

Liquid-phase oxidation of betulin over supported Ag NPs catalysts: Kinetic regularities, catalyst deactivation and reactivation

A. Grigoreva [a], E. Kolobova [a,*], E. Pakrieva [a], P. Mäki-Arvela [b], S. Kuznetsova [a], S.A.C. Carabineiro [c,d], N. Bogdanchikova [e], A. Pestryakov [a], D.Yu. Murzin [b,*]

[a] Research School of Chemistry and Applied Biomedical Sciences, Tomsk Polytechnic University, Lenin Avenue 30, Tomsk 634050, Russia
[b] Johan Gadolin Process Chemistry Centre, Åbo Akademi University, Turku FI-20500, Finland
[c] Centro de Química Estrutural, Institute of Molecular Sciences, Departamento de Engenharia Química, Instituto Superior Técnico, Universidade de Lisboa, Av. Rovisco Pais, Lisboa 1049-001, Portugal
[d] LAQV-REQUIMTE, Department of Chemistry, NOVA School of Science and Technology, Universidade NOVA de Lisboa, Caparica 2829-516, Portugal
[e] Centro de Nanociencias y Nanotecnología, UNAM, Post Box 14, Ensenada 22860, Mexico

ARTICLE INFO

Keywords:
Silver catalyst
Betulin oxidation
Kinetics
Deactivation
Reactivation

ABSTRACT

Betulin, being a pentacyclic triterpene alcohol and an extractive from birch bark, along with its oxo-derivatives, has a broad range of physiological properties of interest for synthesis of pharmaceuticals. Instead of oxidizing betulin with strong and toxic oxidizing agents the present study shows a possibility of using liquid-phase oxidation of betulin with air over supported Ag NPs catalysts as an alternative method for synthesis of its oxo-derivatives. Based on catalytic studies, high resolution transmission electron microscopy, X-ray photoelectron spectroscopy and ultraviolet-visible diffuse reflectance spectroscopy, the evolution of the surface of nano-silver catalysts during the catalysis was demonstrated, as well as under the impact of reactant gas composition. The kinetic regularities and causes of deactivation of supported Ag NPs catalysts were revealed. An approach to the regeneration of silver catalysts was proposed. Kinetic analysis with numerical data fitting was performed resulting in an adequate description of the concentration dependencies.

1. Introduction

Birch bark is a large-tonnage waste of wood processing industry with the share of bark amounting to 10–15% of the total volume of procured wood [1]. It is mainly used as a low-grade fuel, while during its long-term storage, it can become a source of a number of phenolic compounds. The latter are washed out by an atmospheric downfall and melt water, polluting the environment. At the same time, the extractive substances contained in birch bark are valuable initial source to produce bioactive compounds. One the valuable extract is betulin (lup-20 (29)-ene-3, 28-diol, $C_{30}H_{50}O_2$, CAS: 473–98–3) – a pentacyclic triterpene alcohol of the lupane series with the quantities in the bark ranging from 10 to 35% [2,3]. It was counted that a pulp mill producing 200 ktons of birch kraft pulp per year could yield 3000 tons of betulin [4].

Betulin and its oxo-derivatives exhibit a broad range of biological activity and, moreover, can serve as a building block for the synthesis of a new-generation of drugs [5–25]. Separately, it is worth noting some features of betulin as an object of this study. The melting point of betulin ranges from 251 to 261 °C. The functional groups in betulin are the primary and secondary hydroxyl groups and the double bond in the isopropenyl group of the five-membered ring. Betulin undergoes reactions specific to alcohols (esterification, oxidation) as well as those involving the isopropenyl group (isomerization, reduction, oxidation). The specific structure of the ring system of betulin and its derivatives and their functional groups in the positions C-3, C-20 and C-28 stipulate various rearrangements due to intermolecular interactions, depending on the chemical and physical properties of the medium. Betulin has limited solubility in pyridine, tetrahydrofuran, being slightly soluble in most organic solvents and practically insoluble in water. All these features of betulin impose certain restrictions on its oxidation in order to obtain its oxo-derivatives; in particular, there are substantial difficulties with controlling selectivity or in other words excess of oxidation. Currently the main method to produce these derivatives is betulin oxidation using strong and toxic oxidants containing chromium [26,27], manganese [28,29] or a mixture of TEMPO (2,2,6,

* Corresponding authors.
E-mail addresses: ekaterina_kolobova@mail.ru (E. Kolobova), dmurzin@abo.fi (D.Yu. Murzin).

https://doi.org/10.1016/j.mcat.2022.112461
Received 5 April 2022; Received in revised form 9 June 2022; Accepted 19 June 2022
Available online 29 June 2022

6-tetramethylpiperidin-1-oxyl), $NaClO_2$ and NaOCl [28,30]. These approaches are laborious and require complex purification steps, including column chromatography, multiple recrystallization and extraction using large volumes of solvent [31], making their use essentially unfeasible for large scale industrial applications. Thus, there is a need to find alternative methods for synthesis of betulin oxo-derivatives.

One of such methods, proposed by some of the authors of the current work, can be heterogeneous catalytic oxidation of betulin with air over supported nanocatalysts [32–37]. Among the catalysts for liquid-phase oxidation of betulin studied by the authors, the best results were obtained using supported Au NPs catalysts [33]. At the same time it was shown [37] that optimization of the composition and preparation techniques of supported Ag NPs catalysts allowed to achieve performance comparable to nanogold catalysts. As the gold precursors are more expensive, silver catalysts might be a rational alternative to gold ones. Nevertheless, there are several issues related to catalytic behavior of supported Ag NPs catalysts in liquid-phase oxidation of alcohols, which still has to be explored, as only few studies on this topic are available in the scientific literature [38–41], contrary to the widely studied gas-phase oxidation of alcohols over silver [42]. Table 1 shows several examples of the use of silver catalysts for liquid-phase oxidation of alcohols. The main emphasis in Table is placed on the comparison of turnover frequencies (TOF). It should be taken into account, since TOF reflects the maximum number of converted alcohol moles per mole of exposed active Ag sites per unit time, so its value will depend, in addition to Ag amount and its dispersion, also on the alcohol nature, reaction time and conditions. Therefore, TOF is usually calculated at the initial time, when the reaction rate is maximum, since over time, the active surface of the catalyst can change, including deactivation and, accordingly, this will affect both the reaction rate and TOF. Nevertheless, despite the fact that the TOF values presented in Table 1 were calculated after 2 h, it can be said that the alcohol nature, including its spatial and bulk structure, significantly affects the catalyst activity. In addition, as can be seen from the presented data, the nature of the reactant gas also plays an important role. At the same time, according to our knowledge, its impact on active surface of Ag catalysts have not been studied in detail previously. There are also open issues related to studies of kinetic regularities of the liquid phase oxidation, understanding the reasons behind deactivation and developing the procedures for reactivation. Thereby, the present study aims in deeper understanding of the catalytic behavior of supported Ag NPs catalysts in the liquid phase oxidation of betulin.

2. Materials and methods

Based on a previous study, a sample designated as Ag/AlOOH_cal_dp_pH_2 in [37] was selected for a further investigation of kinetic regularities, as well as the origin of deactivation and possible ways of regeneration of nanosilver catalysts during betulin oxidation. This catalyst contains silver nanoparticles (the average size of Ag NPs according to HRTEM was 2.6 nm) deposited by deposition-precipitation with NaOH on pre-calcined boehmite at 600 °C for 3 h (according to XRD data, the support was γ-Al_2O_3), followed by pretreatment of the catalyst in a mixture of 20% H_2 and 80% Ar for 1 h at 300 °C. The silver content in this catalyst, determined by ICP-OES, was 2.8 wt.%. The choice of the catalyst was based on its better catalytic performance (activity and selectivity) compared to other studied supported Ag NPs catalysts [37]. Hereafter, Ag/AlOOH_cal_dp_pH_2 catalyst will be designated as Ag/Al (initial sample).

To identify the effect of reactant gas composition on the catalytic and physicochemical properties of the Ag/Al material, the latter was also pretreated in 100% N_2 (denoted as Ag/Al_pN_2), in a mixture of 21% O_2 and 79% N_2 (denoted as Ag/Al _pO_2(21)) and in 100% O_2 (denoted as Ag/Al_pO_2(100)) at 150 °C for 1 h.

In order to determine the reasons for catalyst deactivation during betulin oxidation, the Ag/Al catalyst after being used in the reaction (i.e., the spent catalysts, denoted as Ag/Al_sp5, Ag/Al_sp30 and Ag/Al_sp360, where the numbers indicate the reaction time in minutes, were separated from the reaction solution, then washed in mesitylene for 4 h at 140 °C, acetone for 2 h at 56 °C and dried under vacuum for 2 h at 80 °C). Ag/Al_sp360 was also tested for betulin oxidation.

In order to assess the possibility of catalytic properties recovery and reuse in betulin oxidation, Ag/Al_sp360 material was pretreated in 20% H_2 and 80% N_2 at 300 °C for 2 h (denoted as Ag/Al_sp360_pH_2), in a mixture of 21% O_2 and 79% N_2 at 500 °C for 3 h, followed by reduction in a mixture of 20% H_2 and 80% N_2 at 300 °C for 2 h (denoted as Ag/Al_sp360_pO_2_pH_2).

The textural properties were assessed by nitrogen adsorption-desorption isotherms at –196 °C, recorded with an ASAP 2060 apparatus (Micromeritics, Norcross, GA, USA). The samples were degassed under vacuum at 300 °C for 5 h before each measurement. The specific surface area (S_{BET}) was determined using the Brunauer-Emmett-Teller (BET) equation applied for the adsorption isotherm (P/P_0 range 0.05–0.25). The Barrett-Joyner-Halenda (BJH) method was applied for

Table 1
Liquid-phase oxidation of alcohols over supported Ag catalysts.

Catalysts	Alcohol	TOF[a], s^{-1}	D	T, °C	Gas reactant	Solvent	Refs.
10%Ag/SiO_2	Benzyl alcohol	0.0009	0.40	130	O_2	Xylene	[43]
10%Ag/SiO_2 + CeO_2 (2:1)	Benzyl alcohol	0.0148	0.40	130	O_2	Xylene	[43]
10%Ag/SiO_2 + CeO_2 (2:1)	Benzyl alcohol	0.0023	0.40	130	air	Xylene	[43]
10%Ag/SiO_2 + CeO_2 (2:1)	Benzyl alcohol	0.0002	0.40	130	N_2	Xylene	[43]
10%Ag/SiO_2 + CeO_2 (2:1)	1-Naphthalenemethanol	0.0039[b]	0.40	130	O_2	Xylene	[43]
1%Ag-MnO_2	Benzyl alcohol	0.0370	0.27	100	O_2	Toluene	[44]
1%Ag-MnO_2	4-Tert-butylbenzyl alcohol	0.0287	0.27	100	O_2	Toluene	[44]
1%Ag-MnO_2	Citronellol	0.0027	0.27	100	O_2	Toluene	[44]
9.56%Ag/GOSH + NHPI	Benzyl alcohol	0.0173	0.09	80	O_2	Acetonitrile	[45]
2.1%Ag/CeO_2/TiO_2	Betulin	0.0013	0.14	140	air	Mesitylene	[34]
2.7%Ag/γ-Al_2O_3_dp_pH_2	Betulin	0.0025	0.33	140	air	Mesitylene	[37]
Ag/Al[c]	Betulin	0.0010	0.38	140	air	Mesitylene	Current study
Ag/Al[c]	Betulin	0.0008	0.38	140	O_2	Mesitylene	Current study
Ag/Al[c]	Betulin	0.0006	0.38	140	N_2	Mesitylene	Current study

GOSH: thiolated graphene oxide.
NHPI: N-hydroxyphthalimide was used as a co-catalyst.
[a] TOF was calculated according to the equation: $TOF = (n_0 - n_{2h})/(n_{Ag}Dt)$, where n_0 - initial number of alcohol moles, n_{2h} - number of alcohol moles after 2 h, n_{Ag} - number of silver moles, D – dispersion, t - time (7200 s).
[b] calculated after 3 h.
[c] silver content– 2.8 wt.%.

the pore size distribution.

X-ray photoelectron spectroscopy (XPS) was applied for a study of the oxidation state of silver using a Thermo Fisher Scientific XPS NEXSA spectrometer with a monochromated Al K-α X-ray source (1486.6 eV) and equipped with a flood gun for the charge compensation. The survey spectra were recorded with a pass energy of 200 eV and a step size of 1 eV, while a pass energy of 50 eV and a step size of 0.1 eV were applied for the high-resolution spectra. The analyzed area was 200 μm^2. Charging shifts were referenced against adventitious carbon at the binding energy (BE) of 285 eV. The CASA XPS software (version 2.3.15, CASA Software Ltd., Teignmouth, UK, http://www.casaxps.com/) was used for processing the spectra. Interpretation of the obtained results was carried out on the basis of the literature data [37,46–54].

High resolution transmission electron microscopic (HRTEM) images (Fig. S1, Supplementary material) were acquired by using a JEM-2100F microscope (JEOL Ltd., Tokyo, Japan) to study the size of silver nanoparticles and their distribution. Before introduction into the instrument, the samples, in a fine powder form, were sonicated in hexane at room temperature, and a drop of the suspension was deposited on a lacey carbon-coated Cu grid. A general survey of the samples was carried out to obtain an image most adequately reflecting the real structure of a sample, thereafter the selected area was scanned at higher resolutions. The particle size for each sample was determined from the analysis of at least 500 particles.

Ultraviolet-visible Diffuse reflectance spectroscopy (UV–vis DRS) was used to confirm the patterns revealed by XPS and HRTEM. UV–vis DR spectra were recorded against a white Spectralon standard in the range of 200–850 nm in 1 nm steps using a Cary 100 SCAN spectrophotometer (Varian, Australia).

It should be noted that for a proper comparative analysis of the results obtained from different methods, namely XPS, HRTEM and UV–vis DRS, as well as catalytic ones, each sample after its preparation, including pre-treatment in various gas mixtures, was not further subjected to any exposure before analysis.

Inductively coupled plasma optical emission spectrometry (ICP-OES) was applied to determine the loading of silver in the initial and spent catalyst using a Horiba Jobin Yvon (Longjumeau, France) Ultima apparatus. Prior to the analysis the solids were dissolved by aqua regia, followed by digested in a microwave oven, diluted and analyzed in the spectrometer.

A procedure for betulin oxidation and the analytical methods for determining changes in the concentration of betulin and its oxidation products during the reaction are described in detail in the previous communications [32–36]. The reaction scheme of betulin oxidation with air over supported Ag NPs catalysts, as well as the main products of its oxidation are shown in Fig. 1. The scheme also includes formation of oligomers and polymeric type of compounds as discussed in [32].

Typically, betulin and the catalyst were mixed in mesitylene (total solution volume 100 mL) and the reactant gas was bubbled through the liquid (flow rate 50 mL min^{-1}) at a certain temperature under constant stirring (500 rpm). Kinetic experiments were performed in the temperature range of 80–140 °C using 0.05 – 0.4 g catalyst and the initial betulin concentration varied from 1.13 mmol/L – 9.04 mmol/L. In addition, the oxygen content in the gas atmosphere was changed from 0% to 100% by adjusting the oxygen level with nitrogen (Table 2).

It should be noted in this section that without the catalyst, the betulin conversion for 6 h was only 4%. In order to exclude the possible course of betulin oxidation without the catalyst, as well as homogeneous catalysis, resulting from the leaching of silver from the catalyst surface during betulin oxidation, the following catalytic tests were performed: 1. 0.2 g of betulin was dissolved in 100 mL of mesitylene (the initial concentration of betulin was 4.52 mmol/L), then the solution was heated to 140 °C and bubbled with air (flow rate 50 mL min−1) for 6 h with constant stirring (500 rpm); 2. 0.2 g of betulin was dissolved in 100 mL of mesitylene (the initial concentration of betulin was 4.52 mmol/L), then 0.2 g of the catalyst was added, further the solution was heated to 140 °C under constant stirring (500 rpm) and air was bubbled through

Table 2
The values of experimental variables (temperature, catalyst loading, initial betulin concentration and oxygen content).

Entry	T (°C)	$m_{catalyst}$ (g)	$C_{0,Betulin}$ (mmol/L)	Oxygen content (%)
1	140	0.05	4.52	21
2	140	0.1	4.52	21
3	140	0.2	4.52	21
4	140	0.4	4.52	21
5	80	0.2	4.52	21
6	100	0.2	4.52	21
7	120	0.2	4.52	21
8	140	0.2	4.52	0
9	140	0.2	4.52	12
10	140	0.2	4.52	17
11	140	0.2	4.52	30
12	140	0.2	4.52	48
13	140	0.2	4.52	100
14	140	0.2	1.13	21
15	140	0.2	2.60	21
16	140	0.2	3.39	21
17	140	0.2	6.78	21
18	140	0.2	9.04	21

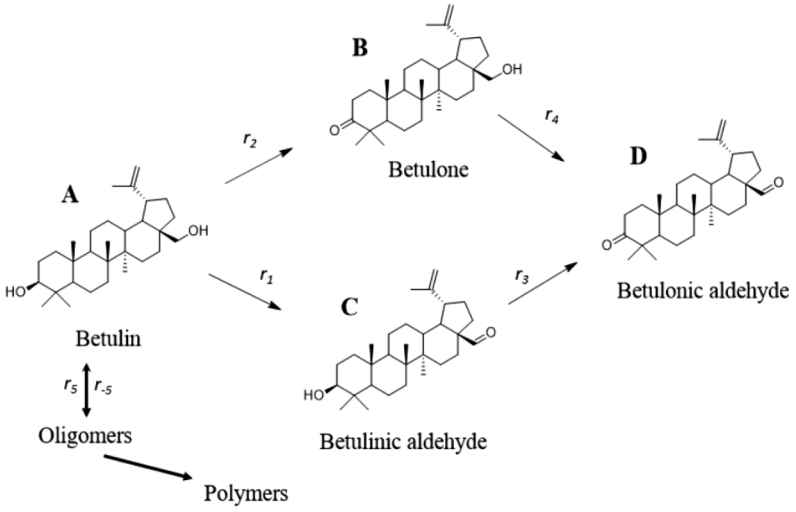

Fig. 1. The reaction scheme for betulin oxidation with air over supported Ag NPs catalysts.

the liquid (flow rate 50 mL/min) until a betulin conversion of 20% is achieved. After that, the hot solution was filtered to separate the catalyst, and then the betulin oxidation was continued under the same conditions, but without the catalyst. To minimize the limitations of mass and heat transfer, catalyst particles with a size of 50 μm and a high stirring rate of 500 rpm were used. Additionally, an experiment was carried out with a catalyst particle size of ca. 100 μm.

The samples were withdrawn from the reaction medium at regular intervals and analyzed on a Crystallux-4000 M Meta-chrome gas chromatograph (Yoshkar-Ola, Russia) equipped with an Agilent HP-1 (Santa-Clara, CA, USA) capillary column. Silylation of the samples by a mixture of pyridine, N,O-bis(trimethylsilyl)trifluoroacetamide and trimethylsilyl chloride (1:4:1 vol ratio) was followed by heating in an oven (70 °C for 45 min) prior to GC-analyses. It should be noted that silylation prior to GC analysis was used to obtain volatile derivatives of non-volatile compounds (betulin and its oxo-derivatives) and to achieve a lower detection limit of the analyzed substances.

The TOF values were calculated as the number of converted betulin moles per mole of exposed active Ag site per unit time, according to the following equation:

$$TOF = \frac{n_{Betulin}}{n_{Ag} D t} \quad (1)$$

where $n_{Betulin}$ is the number of converted betulin moles, n_{Ag} is the number of silver moles, D is dispersion and t is a time equal to 900 s. The dispersion was calculated based on the average size of Ag NPs determined by HRTEM.

3. Results and discussion

Table 3 summarizes the results of kinetic studies, reporting the values of the initial rates (calculated for the first 5–15 min), TOF, betulin conversion, yields of the reaction products and the mass balance closure depending on the change of one of the four experimental parameters: catalyst loading (0.05 - 0.4 g), temperature (80 - 140 °C), oxygen concentration in nitrogen (0 - 100%) and the initial betulin concentration (1.13 - 9.04 mmol/L). The influence of each parameter will be discussed below in detail.

3.1. Effect of initial betulin concentration

Fig. 2a shows the change in the initial rate calculated from the products formed in the range from 5 to 15 min, depending on the initial concentration of betulin. As can be seen from the presented data, the initial rate increases with an increase in the initial betulin concentration up to 3.39 mmol/L, passing thereafter through a maximum. This behavior of the experimental curve is similar to the kinetic regularities observed for reactions proceeding according to the Langmuir-Hinshelwood mechanism. Namely, at low concentrations of betulin, the degree of surface coverage with betulin is low, and all chemisorbed betulin molecules can react with chemisorbed oxygen molecules. The reaction rate increases to a maximum value at which the degree of surface coverage with betulin is equal to the degree of surface coverage with oxygen. With a further increase in the betulin concentration, the surface is increasingly occupied by betulin, and the probability of reacting chemisorbed molecules of betulin and oxygen being located on neighboring centers decreases, and as a result, also the reaction rate.

The TOF value also increases to the initial betulin concentration of 3.39 mmol/L, then it decreases (Table 3, entries 3,14–18). At the same time, for initial betulin concentrations of 6.78 and 9.04 mmol/l, the TOF values are equal (Table 3, entries 17 and 18), and higher than for 4.52 mmol/L (Table 3, entry 3).

Betulin conversion decreases almost linearly with an increase in the initial concentration of betulin (Table 3, entries 3,14–18), while the mass balance closure expressed through GCLPA (closure in the liquid phase balance by GC analysis) has the opposite dependence (Table 3, entries 3,14–18). For simple first-order reactions, the conversion does not depend on the initial concentration of the reactant and is determined only by the reaction time. At the same time, the mathematical description for the first-order kinetics does not take into account the reaction mechanism. Deviations from the first order of the reaction indicate a complex course of the process. Possible reasons for the deviation may be the occurrence of sequential/parallel/opposite reactions, leading to a change in the order and mechanism of the reaction. In the current case, both sequential (oxidation of betulone (B) and betulinic aldehyde (C) to betulonic aldehyde (D)) and parallel reactions (polymerization/oligomerization and esterification) take place, explaining the observed deviation from the kinetic regularities for first-order reactions. Herewith an increase in the GCLPA with an increase in the initial concentration of

Table 3
The initial reaction rate (r_0) calculated from formation of all products visible in GC analysis between 5 and 15 min, TOF calculated according to Eq. (1) during the first 15 min, liquid phase mass balance determined by GC analysis (GCLPA), betulin conversion after 6 h (X), Y_B, Y_C, Y_D - yield of betulone (B), betulinic (C) and betulonic (D) aldehydes, respectively.

Entry	T (°C)	$m_{catalyst}$ (g)	$C_{0,Betulin}$ (mmol/L)	Oxygen content (%)	$r_0 \times 10^{-3}$ (mmol/min/g_{cat})	TOF (s^{-1})	GCLPA (%)	X (%)	Y_B (%)	Y_C (%)	Y_D(%)
1	140	0.05	4.52	21	0.05	0.0033	97	5	<1[a]	1[a]	1[a]
2	140	0.1	4.52	21	1.35	0.0032	96	8	<1[a]	2[a]	4[a]
3	140	0.2	4.52	21	9.58	0.0043	90	54	5[b](3[c])	7[b](7[c])	29[b](25[c])
4	140	0.4	4.52	21	3.63	0.0045	72	89	2[b]	5[b]	15[b]
5	80	0.2	4.52	21	0.02	0.0030	87	13	<1[a]	<1[a]	<1[a]
6	100	0.2	4.52	21	0.26	0.0030	87	13	<1[a]	1[a]	1[a]
7	120	0.2	4.52	21	1.37	0.0032	90	17	<1[a]	3[a]	5[a]
8	140	0.2	4.52	0	1.49	0.0024	96	45	4[c]	8[c]	23[c]
9	140	0.2	4.52	12	5.95	0.0039	91	60	4[c]	6[c]	23[c]
10	140	0.2	4.52	17	12.46	0.0053	90	56	4[c]	6[c]	23[c]
11	140	0.2	4.52	30	7.50	0.0042	90	55	4[c]	5[c]	24[c]
12	140	0.2	4.52	48	5.82	0.0040	92	53	4[c]	7[c]	23[c]
13	140	0.2	4.52	100	4.47	0.0038	92	39	3[a]	7[a]	24[a]
14	140	0.2	1.13	21	2.38	0.0028	64	93	2[b]	5[b]	11[b]
15	140	0.2	2.26	21	3.80	0.0047	72	85	2[b]	5[b]	12[b]
16	140	0.2	3.39	21	12.54	0.0064	79	64	3[b]	6[b]	21[b]
17	140	0.2	6.78	21	7.98	0.0052	91	26	<1[a]	3[a]	14[a]
18	140	0.2	9.04	21	2.70	0.0052	93	17	<1[a]	3[a]	7[a]

[a] yield after 6 h.
[b] yield at 50% of betulin conversion.
[c] yield at 40% of betulin conversion.

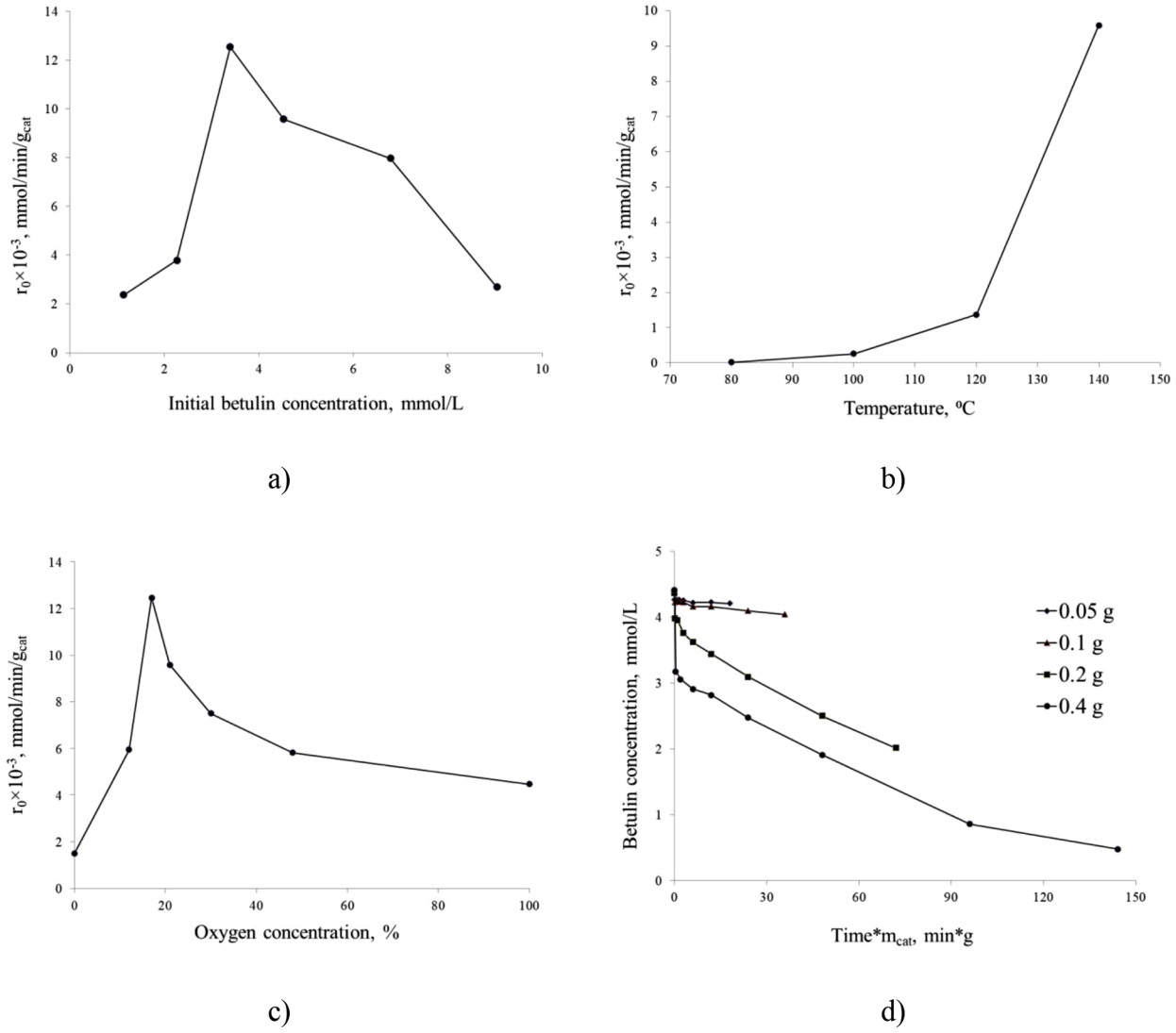

Fig. 2. Betulin oxidation over Ag/Al catalyst. The initial reaction rates for formation of products between 5 and 15 min in betulin oxidation as a function of: (a) the initial betulin concentration, (b) temperature, (c) O_2 concentration in the reactant gas. (d) Concentration of betulin as a function of normalized time (time multiplied by catalyst mass).

betulin seems to be associated with a decrease in the available specific surface area compared to the amount of betulin.

It can be noted that regardless of the initial concentration of betulin, the main product of its oxidation is betulonic aldehyde (D), followed by betulinic aldehyde (C) and betulone (B), respectively (Table 3, entries 3,14–18). Since the initial concentration of betulin predetermines its conversion and the GCPLA, and accordingly, it also affects the yields of products. The yields of the products increase up to the initial betulin concentration of 4.52 mmol/L, following by their decline (Table 3, entries 3,14–18).

3.2. Effect of catalyst loading

In the absence of catalyst deactivation or without the effect of gas/liquid mass transfer limitations, the curves describing the dependence of the substrate concentration on the normalized time (i.e. time multiplied by the mass of the catalyst) should coincide [33,55–57]. An experiment using a catalyst (Ag/Al) with different particle sizes, namely 50 and 100 μm, showed that the betulin conversion in the first and second cases is very close and amounts to 54 and 58%, respectively. Thereby, it can be assumed that in the present study, the impact of limitations caused by gas/liquid mass transfer is negligible. At the same time, the highest betulin conversion and TOF were achieved using the largest amount of catalyst (Fig. 2d, Table 3, entries 1–4), which indicates the presence of catalyst deactivation. Herewith the catalyst deactivation was less pronounced when using the largest catalyst loading due to the higher available surface area per the amount of betulin.

Possible reasons for the catalyst deactivation can be: impurities in the used reagents, silver leaching, sintering of silver nanoparticles and/or change in the electronic state of silver, an alteration of the textural properties of the catalyst surface, strong adsorption of the substrate/products or side products on the catalyst surface, as well as blocking of the pores by coke.

In our previous study [32], it was found that oligomeric and polymeric structures with molecular weights of 1000 and 5000 Da are formed on the catalyst surface during betulin oxidation with synthetic air over Au NPs catalysts. Formation of these structures was responsible for the mass imbalance between the theoretical values of GCLPA (100%) and the experimentally measured ones, and their strong adsorption on the catalyst surface was considered as one of the reasons for catalyst deactivation. In our subsequent studies [33,37], the value of the mass balance closure (GCPLA) was considered as description of deactivation, indicating occurrence of the side reactions of oligomerization, polymerization and/or esterification. In the current study, the mass balance

closure decreases with the increasing catalyst loading (Table 3, entries 1–4). Comparing the values of GCPLA, betulin conversion and product yields, it can be assumed that the contribution of side reactions increases with increasing catalyst loading (Table 3, entries 1–4). At the same time no new substances were found during GC analysis, thereby indicating formation of products with a higher molecular weight. Thus, the strong adsorption of such compounds on the catalyst surface may be one of the reasons for its deactivation.

Analyzing the effect of catalyst loading on the yield of betulone (B), betulinic (C) and betulonic (D) aldehydes (Table 3, entries 1–4), it can be said that they increase up to a catalyst loading of 0.2 g, then, due to the occurrence of side reactions, blocking part of the active surface of the catalyst, the yields decrease, despite an increase in betulin conversion. A similar effect of the catalyst loading on the yield of products was previously observed for the betulin oxidation over supported Au NPs catalysts [33]. In all cases, the main product of betulin oxidation is betulonic aldehyde (D), then betulinic aldehyde (C) and betulone (B) (Table 2, entries 2–4), except for 0.05 g of catalyst (Table 3, entry 1).

3.3. Effect of temperature

The effect of temperature on the initial rate of the betulin oxidation is clearly demonstrated in Fig. 2b. The initial reaction rate, TOF, betulin conversion, and yields of betulone (B), betulinic (C) and betulonic (D) aldehydes increase with increasing reaction temperature (Fig. 2b, Table 3, entries 3, 5–7). In this case, the mass balance closure is weakly dependent on temperature and varies in the range 87–90% (Table 3, entries 3, 5–7).

The activation energies of the formation of betulone (B), betulinic (C) and betulonic (D) aldehydes were determined according to the Arrhenius equation using the initial rate for formation of betulone (B), betulinic (C) or betulonic (D) aldehydes between 5 and 15 min.

The activation energy for betulone (B), betulinic (C) and betulonic (D) aldehydes formation calculated from the slope of the Arrhenius plot was found to be 44, 183 and 101 kJ/mol, respectively. For comparison, the activation energy of betulone formation in betulin oxidation with synthetic air over Au NPs catalyst was previously reported to be 38 kJ/mol [33]. The obtained values of activation energy explain why the main product of betulin oxidation over supported Ag NPs catalysts is betulonic aldehyde (D), formed as a result of betulone (B) oxidation.

3.4. Effect of O_2 concentration

Fig. 2c shows dependence of the initial rate of the betulin oxidation on the oxygen concentration in the reactant gas (from 0 to 100% in nitrogen). The highest initial reaction rate was observed when the oxygen content in the reactant gas was 17 vol.%; with an increase or decrease in the oxygen concentration in the reactant gas, a decrease in the initial reaction rate was observed (Fig. 2c, Table 3 entries 3, 8–13). As in the case of a change in the initial betulin concentration (reagent I), a change in the concentration of oxygen (reagent II) in the reactant gas leads to a curve typical for the Langmuir-Hinshelwood mechanism. This is, however, a special type of the Langmuir-Hinshelwood mechanism, as adsorption of oxygen on silver is accompanied by its dissociation [58, 59], while at a high coverage, non-dissociative (molecular) adsorption of oxygen takes place [60]. Furthermore, in the surface layers of silver, oxygen dissolves in the metal in the form of strongly bound atomic oxygen replacing silver atoms in the fcc lattice of the metal and/or surface oxygen penetrating into the octahedral holes of the near-surface layers of the fcc silver lattice [61–63]. The possibility of the existence of two forms of atomically adsorbed oxygen on the silver surface was substantiated in [58,63]: (1) oxyradical, equivalent to the electrophilic state of adsorbed oxygen, and (2) oxide, considered as the nucleophilic state of oxygen. Electrophilic oxygen is absorbed directly on the silver surface and resembles oxygen in AgO in terms of its properties. Formation of this state occurs without reconstruction of the silver surface. The formation of the nucleophilic state of oxygen is directly related to the reconstruction of the silver surface. The nature of the Ag-O bond in this case is close to the bond in bulk oxide Ag_2O and high ionicity of the Ag-O bond ensures the transition of silver atoms to the ionic form Ag^+. Taking into account all the presented above features of the oxygen interactions with the silver surface, it is obvious that in this case the mechanism of oxygen adsorption on the catalyst surface is more complex than in the classical representation of the Langmuir-Hinshelwood mechanism.

The dependence of TOF on the oxygen concentration in the reactant gas is similar to the corresponding dependence for the initial reaction rate (Fig. 2c). That is, the TOF value increases to the oxygen concentration of 17 vol.%, followed by its decrease with increasing oxygen concentration (Table 3 entries 3, 8–13).

The betulin conversion slightly depends on the O_2 concentration in the reactant gas in the range of 17–48 vol.% (Table 3, entries 3, 10–12), while the highest conversion of betulin was achieved at an oxygen concentration of 12 vol.% (Table 3, entry 9), at the same time its lowest values were obtained for neat nitrogen and oxygen (Table 3, entries 8,13). The mass balance closure mildly depends on the concentration of oxygen in the reactant gas, namely in the range from 12 to 100 vol.% O_2 GCPLA varies between 90 and 92% (Table 3, entries 3, 9–13). At the same time, the highest mass balance closure (96%) was observed when using 100% nitrogen as a reactant gas (Table 3, entry 8). At the same level of betulin conversion, the yields of betulone (B), betulinic (C) and betulonic (D) aldehydes vary within 3–4, 5–8 and 23–25%, respectively (Table 3, entries 3, 8–13). Thus, the yields of betulin oxidation products insignificantly depend on the oxygen concentration in the reactant gas. In all cases, the main reaction product was betulonic aldehyde (D), followed by betulinic aldehyde (C) and betulone (B).

For in depth understanding of the observed influence of the oxygen concentration in the reactant gas on the catalytic behavior of supported Ag NPs catalysts, a number of additional physicochemical studies were carried out. In particular, in order to simulate the reaction conditions and thereby find out what happens to the catalyst under the action of a reactant gas of different compositions, the initial sample (Ag/Al) was pretreated in different ways (air, neat O_2 or neat N_2) at 150 °C for 1 h. Then, the changes in the electronic state of silver, size and distribution of Ag NPs on the support surface were evaluated.

Based on the data presented in Fig. 3, one can clearly trace how the electronic state and the average size of Ag NPs change under the influence of the pretreatment atmosphere/reactant gas composition. According to XPS data, in the initial sample (Ag/Al), the fraction of silver in the metallic state was 94% (also taking into account 25% of silver in the form of silver clusters (Ag_n^0) with size below 2 nm), while the average size of Ag NPs was 2.6 nm (Fig. 3a) [37]. After the Ag/Al material was subjected to subsequent treatment in a nitrogen atmosphere at 150 °C for 1 h, the amount of silver in the metallic state did not change (taking into account also 16% of silver in the form of silver clusters (Ag_n^0) with size below 2 nm), however, the average size of Ag NPs changed to 6.5 nm (Fig. 3b). In the case when the Ag/Al material was pretreated in air or in 100% O_2 at 150 °C for 1 h, the amount of silver in the metallic state decreased to 57 and 40%, and the average size of Ag NPs increased to 4.7 and 27.1 nm, respectively (Fig. 3c, d). Separately, it should be noted that despite the fact that the mean size of silver NPs for Ag/Al_pO_2(100) was 27.1 nm, 23% of silver particles on its surface still have a size lower than 3 nm (Fig. 3d). For the initial catalyst, as well as pretreated in air and neat nitrogen, these values were 92, 52 and 25%, respectively (Fig. 3a–c). Thus, additional treatment of Ag/Al catalyst in an atmosphere of nitrogen, oxygen, or their mixture of 21% O_2 and 79% N_2, leads to an increase in the average size of Ag NPs. At the same time, it should be noted that the pretreatment of Ag/Al catalyst in air or neat O_2, along with an increase in the average NP size, also results in a decrease in the fraction of silver in the metallic state. These results show that the composition of the reactant gas significantly affects the physicochemical properties of silver catalysts under the studied conditions (the electronic

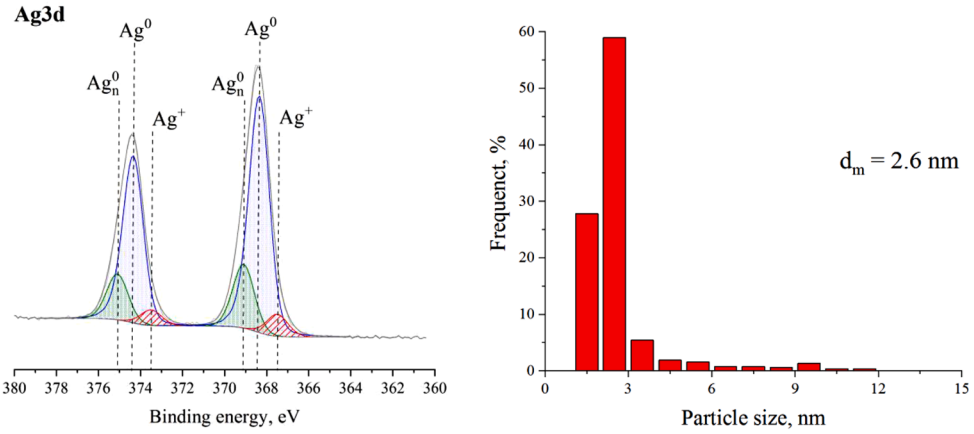

Ag^0 - 69%, Ag^0_n - 25%, Ag^+ - 6%

NPs with size below 3 nm - 92%

a)[a]

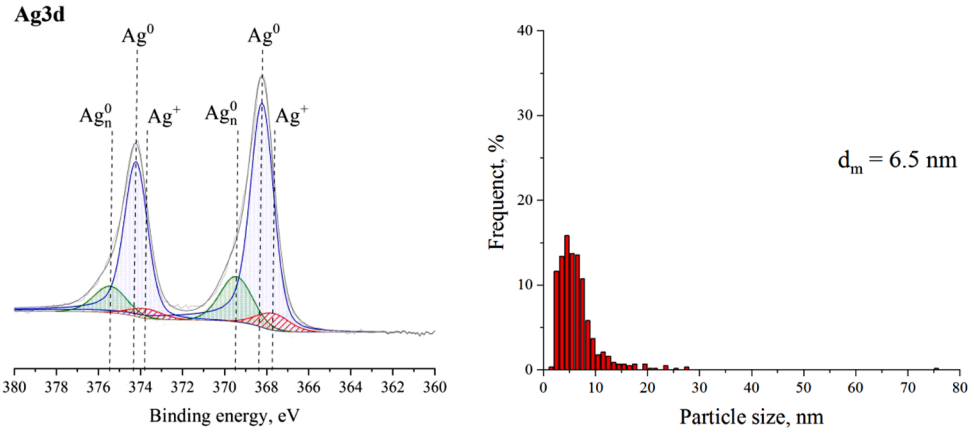

Ag^0 - 78%, Ag^0_n - 16%, Ag^+ - 6%

NPs with size below 3 nm - 25%

b)

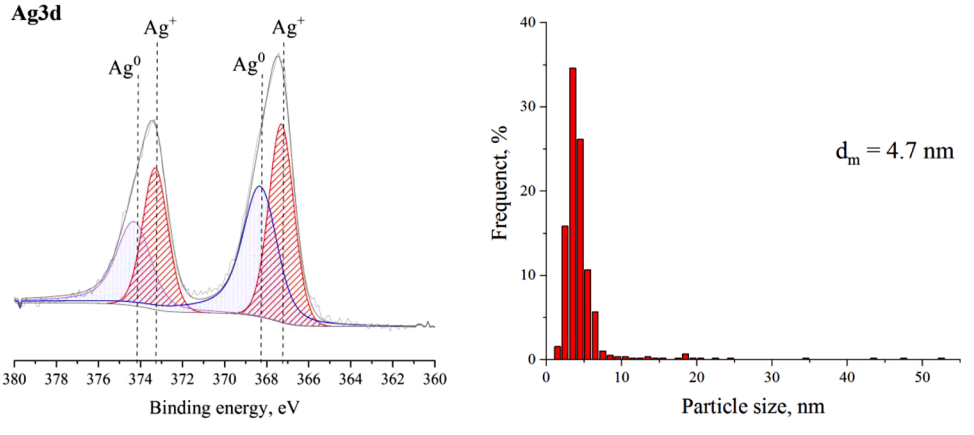

Ag^0 - 57%, Ag^+ - 43%

NPs with size below 3 nm - 52%

c)

Fig. 3. Ag3d XPS and Ag particles distribution for: (a) Ag/Al[a]; (b) Ag/Al_pN_2; (c) Ag/Al_pO_2(21); (d) Ag/Al_pO_2(100); (e) Ag/Al_sp5; (f) Ag/Al_sp30; (g) Ag/Al_sp360; (h) Ag/Al_sp360_pH_2; (i) Ag/Al_sp360_pO_2_pH_2. [a]Data from [37].

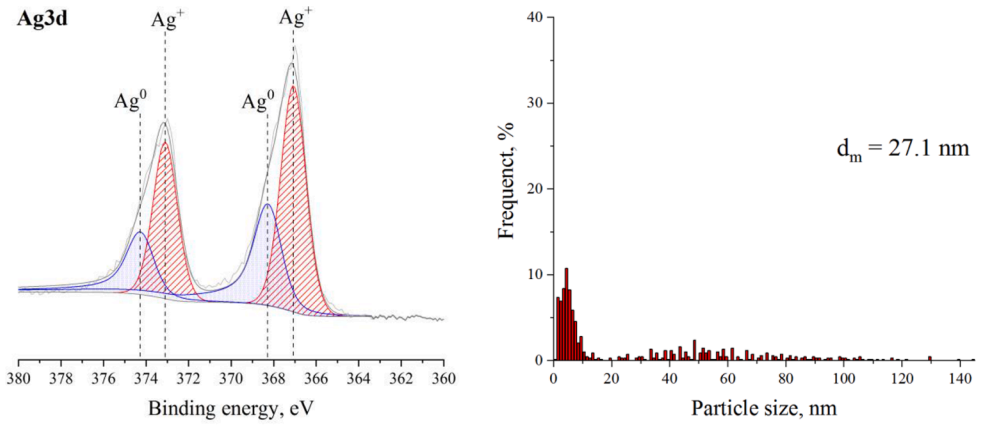

Ag^0 - 40%, Ag^+ - 60%

NPs with size below 3 nm - 23%

d)

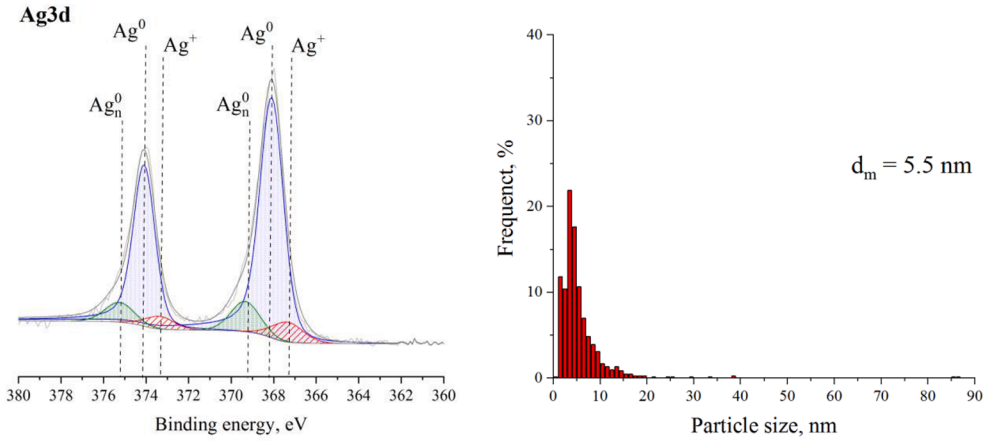

Ag^0 - 83%, Ag^0_n - 11%, Ag^+ - 6%

NPs with size below 3 nm - 44%

e)

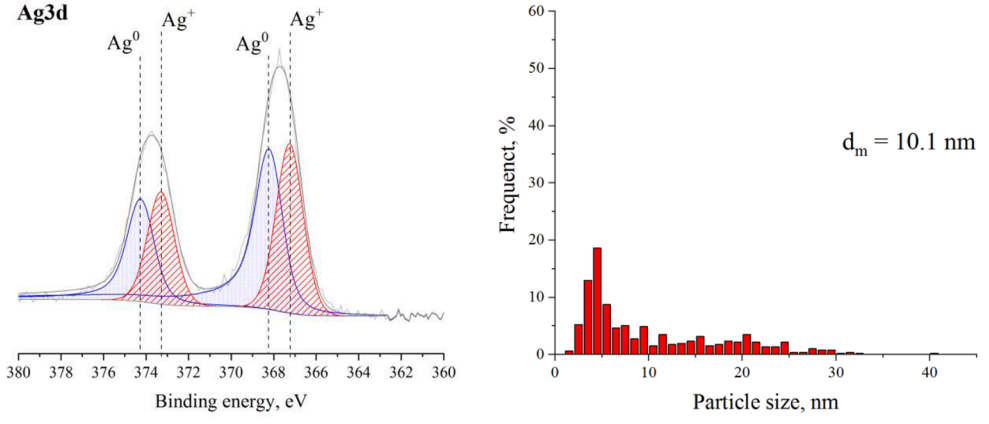

Ag^0 – 60%, Ag^+ - 40%

NPs with size below 3 nm - 19%

f)

Fig. 3. (*continued*).

state of silver, the size and distribution of Ag NPs on the support surface), reflecting complexity of oxygen interactions with silver. The features of these interactions are also visible in the catalytic properties of silver catalysts (Fig. 2b, Table 3, entries 3, 8–13).

Further in order to understand how the electronic state of silver and the average size of Ag NPs change during the catalytic process, the catalysts were studied by XPS and HRTEM after 5, 30, and 360 min of betulin oxidation with air at 140 °C (Fig. 3e, f, g). As can be seen from the

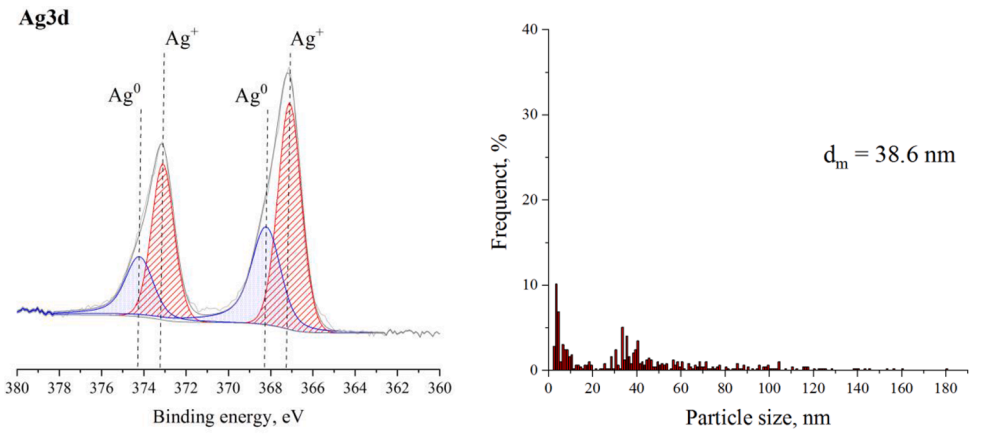

Ag^0 - 42%, Ag^+ - 58%

NPs with size below 3 nm - 13%

g)

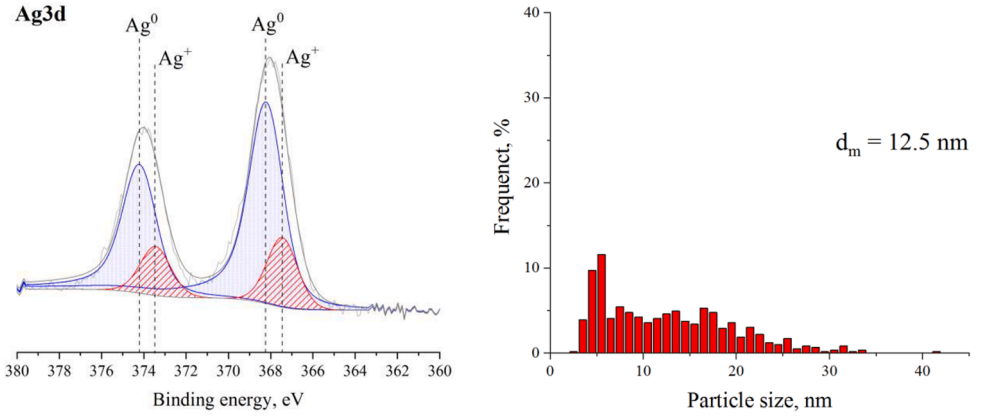

Ag^0 - 80%, Ag^+ - 20%

NPs with size below 3 nm - 4%

h)

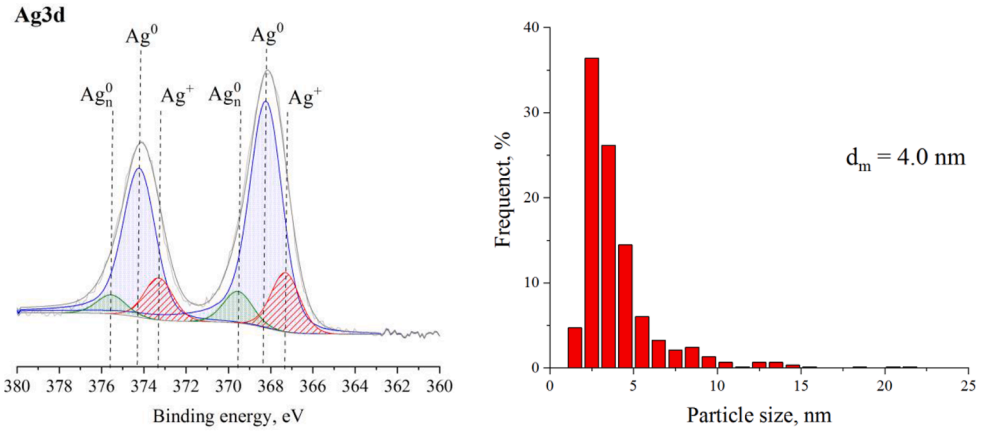

Ag^0 - 78%, Ag^0_n - 7%, Ag^+ - 15%

NPs with size below 3 nm - 56%

i)

Fig. 3. (*continued*).

data presented in Fig. 3e, after 5 min of the reaction, the average size of Ag NPs reaches 5.5 nm, while this value was 2.6 nm for the sample before the reaction (Ag/Al, Fig. 3a). At the same time, the fraction of silver in the metallic state remained at 94% (taking into account 11% of silver in the form of silver clusters (Ag^0_n) with size below 2 nm). After 30 min of the reaction, the fraction of metallic silver decreased to 60%, and the average size of Ag NPs reached 10.1 nm (Fig. 3f). These values for the sample after 360 min (Ag/Al_sp360) (Fig. 3g) were 42% and 38.6

nm, respectively.

The observed patterns in the change of the average size of Ag NPs and its electronic state under the influence of the pretreatment atmosphere/reactant gas composition and reaction conditions are also confirmed by UV–vis DRS (Fig. 4). Absorption at 277 nm corresponds to the charge transfer band in $Ag_n^{\delta+}$ clusters (n = 2–7) [64–70], while the absorption band at 320 nm is associated with large aggregates of silver particles and/or a surface film of silver (interzonal transitions of electrons and the intrinsic photoelectric effect) [71]. The intensity of the absorption bands at 277 and 320 nm increases after the reaction for (Ag/Al_sp360), as well as after changing from neat nitrogen (Ag/Al_pN_2) to neat oxygen (Ag/Al_pO_2(100)). This is due to partial oxidation of metal clusters and aggregation of silver particles upon the treatment and exposure to the reaction conditions. The plasmon resonance signal (450–470 nm) corresponding to the metal particles of a certain size was not observed in the UV–vis DR spectra of the studied materials.

The above results demonstrate the evolution of silver catalysts surface under the impact of pretreatments/composition of the reactant gas (0 - 100% of oxygen in nitrogen) and during catalysis (air - reactant gas, temperature - 140 °C, mesitylene - solvent, betulin - substrate). A comparison of the obtained results with the literature data is not straightforward. In fact, there are almost no studies dealing with the exploration of silver catalysts for the liquid-phase oxidation of organic substrates with oxygen or air, including alcohols [38,39]. Moreover, the reaction conditions used in current study are different, in particular the process temperature (140 °C), which is on average 40–80 °C higher than typically used for liquid-phase oxidation of most common alcohols. The paper [72] considers issues related to the influence of temperature on the agglomeration of metals and oxides from the point of view of the driving forces of dissociation and diffusion of surface atoms. With an increase in temperature, the lattice vibration of surface atoms increases, reaching the Hüttig temperature (0.3 of the melting temperature), and the surface atoms in the places of defects (edges, corners, etc.) can dissociate and diffuse over the surface. When the Tamman temperature (0.5 of the melting temperature) is reached, the bulk atoms also become mobile. Taking into account that the Hüttig and Tamman temperatures for metallic silver are 97 and 344 °C, respectively, it can be assumed that at the temperature of betulin oxidation (140 °C), dissociation and surface diffusion of only weakly bound surface silver atoms can occur. Under the impact of pretreatments/composition of reactant gas or reaction conditions, in particular air or neat oxygen, the electronic state of silver changes, namely, part of the metallic silver is oxidized to silver oxide (Fig. 3). The latter has the Hüttig and Tamman temperatures equal

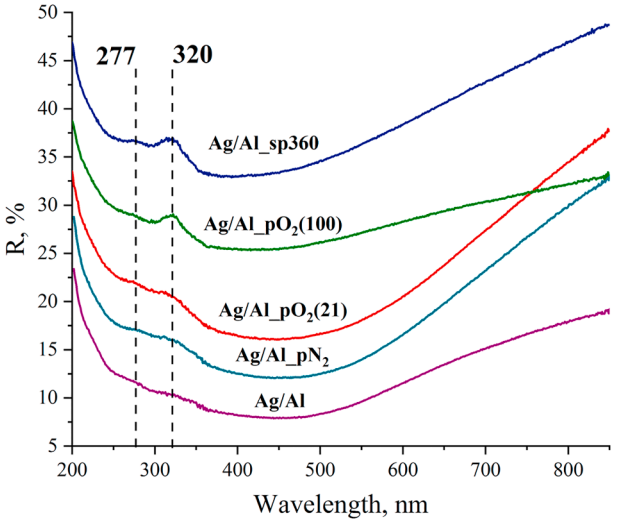

Fig. 4. UV–vis DR spectra of Ag catalysts: Ag/Al (purple); Ag/Al_pN_2 (cyan); Ag/Al_pO_2(21) (red); Ag/Al_pO_2(100) (green); Ag/Al_sp360 (dark blue).

to 84 and 140 °C, respectively. It can be assumed that agglomeration of silver observed in the current study during catalytic process can occur as a result of a change in the electronic state of silver. This is followed by surface diffusion, collision and coalescence of silver oxide with the subsequent formation of larger silver particles. In addition, as postulated in [73], on the surface of silver catalysts with an average size of Ag NPs lower than 3 nm, contains a high fraction of low-coordinated Ag atoms, promoting the adsorption and dissociation of oxygen molecules, which ultimately leads to the oxidation of small metal NPs. Taking into account that in the initial catalyst (Ag/Al), the fraction of Ag NPs lower than 3 nm is 92% (Fig. 3a), accordingly, in the current case, oxidation of the metal particles is fast, while an oxidizing environment (air) is likely to prevent a fast reverse transition of silver oxide into silver metal. Thereby, the $Ag^0 \leftrightarrow Ag^+$ equilibrium is altered, and a relatively high temperature (140 °C) promotes the diffusion of silver oxide over the catalyst surface.

When Ag/Al_sp360 was reused in betulin oxidation, the betulin conversion reached only 2% and TOF decreased by 11 fold (Table 4, entry 2), which indicates almost complete deactivation of the catalyst in the first reaction cycle. To understand the origin of catalyst deactivation, Ag/Al_sp360 was pretreated in a mixture of H_2 in nitrogen at 300 °C for 1 h and studied in betulin oxidation (Table 4 entry 3). As can be seen from Table 4, the conversion of betulin and TOF for Ag/Al_sp360_pH_2 were only 5% and 0.0006 s^{-1}, respectively, while the average size of Ag NPs and the fraction of the metallic silver for this sample were 12.5 nm and 80%, respectively (Fig. 3h, Table 4, entry 3). Thus, it is obvious that the average size of Ag NPs and the fraction of the metallic silver are not the only factors determining deactivation of the supported Ag NPs catalysts in betulin oxidation. Another determining factor can be strong adsorption of the substrate/products or side products on the catalyst surface, while the high-temperature treatment of the catalyst in the mixture 20% H_2 + 80% N_2 at 300 °C leads, most likely, to carbonization of the catalyst surface. This assumption was confirmed by the XPS analysis of this material, for which the carbon content increased 2.3 fold compared to the initial catalyst (Ag/Al). Deactivation by strong adsorption of the substrate/products or coking is also evidenced by kinetic data (Fig. 2a,d). In addition, the specific surface area (S_{BET}), the average size and the pore volume for Ag/Al_sp360, being respectively 190 m^2/g, 5.8 nm and 0.38 cm^3/g confirmed pore blocking as the corresponding values for the starting material (Ag/Al) were 249 m^2/g, 6.3 nm and 0.50 cm^3/g, respectively [37]. Another evidence of strong adsorption of organic deposits on the Ag/Al_sp360 surface is the appearance of CO_2 in the reaction products during the pretreatment of this sample in a mixture of 21% O_2 and 79% N_2 at 500 °C for 3 h. After a sequential treatment of Ag/Al_sp360, first in a mixture of 21% O_2 and 79% N_2 at 500 °C for 3 h, then in a mixture of 20% H_2 and 80% N_2 at 300 °C for 2 h, betulin conversion and TOF for this catalyst were 41% and 0.0042 s^{-1}, respectively (Table 4, entry 4). In addition, for Ag/Al_sp360_pO_2_pH_2, the average size of Ag NPs and the contribution of metallic silver were 4.0 nm and 85%, respectively (Table 4, entry 4; Fig. 3i). Separately, it should be noted that, according to the XPS results, no extraneous elements were detected on the surface of the studied materials, indicating absence of catalytic poisons in the used reagents, ruling out poisoning as the cause of catalyst deactivation. In addition, elemental analysis by ICP-OES showed that the silver loading for the spent catalyst (2.5 wt.%) decreased by only 10% compared to the initial one (2.8 wt.%), being within the error of the method. Subsequently, leaching even if present, cannot account for severe deactivation. This is also confirmed by hot-filtration experiment. After removing the catalyst from the reaction media, no further increase in betulin conversion was observed.

Thus, it can be concluded that deactivation of the supported Ag NPs catalyst in the oxidation of betulin has a cumulative character and was caused by an increase in the average size of Ag NPs, a decrease in the fraction of metallic silver, and strong adsorption of the substrate/products on the catalyst surface as well as coking. Separately, it is worth

Table 4
Influence of the reaction conditions on the catalytic, structural, and electronic characteristics of supported Ag NPs catalysts.

Entry	Catalyst	$r_0 \times 10^{-3}$ (mmol/min/g_{cat})	TOF (s^{-1})	X (%)	GCLPA (%)	Y_B (%)	Y_C (%)	Y_D (%)	Ag average particle size (nm) by HRTEM	Fraction of Ag in the metallic state (%) by XPS
1	Ag/Al	9.58	0.0043	54	90	3	7	25	2.6	94
2	Ag/Al_sp360	0.23	0.0004[a]	2	99	<1	1	<1	38.6	42
3	Ag/Al_sp360_pH_2	0.63	0.0006[a]	5	99	<1	1	3	12.5	80
4	Ag/Al_sp360_pO_2_pH_2	4.61	0.0042[a]	41	89	2	5	23	4.0	85

r_0 - the initial rate calculated from formation of products between 5 and 15 min (mmol/min/g_{cat}); X - conversion of betulin after 6 h (%); GCLPA (the mass balance closure) - the sum of reactant and product masses in GC analysis after 6 h (%); Y_B, Y_C and Y_D - yield of betulone (B), betulinic (C) and betulonic (D) aldehydes at 40% conversion (%), except for Ag/Al_sp360 and Ag/Al_sp360 _pH_2, for which the yields are presented at maximum conversion of 2 and 5%, respectively. Conditions: 140 °C, air (50 mL/min) as oxidant, solvent - mesitylene, initial betulin concentration - 4.5 mmol/L, 0.2 g of catalyst. [a]TOF was calculated on the assumption that silver particles with a size of 3 nm are active, as previously revealed in [37].

noting that coke in this case refers to individual fragments of adsorbed molecules that can also be broken down to carbon. Accordingly, taking into account the adsorption of the substrate/products/byproducts on the catalyst surface, the presence of coke cannot be excluded. A possible way to reactivate the catalyst can be sequential pretreatment first in a mixture of 21% O_2 and 79% N_2 (air) at 500 °C for 3 h, and then in a mixture of 20% H_2 and 80% N_2 at 300 °C for 2 h.

3.5. Kinetic analysis

Kinetic analysis of betulin oxidation over Ag/Al catalyst was done followed the previous work of the authors [32] where a network comprising formation of oligomers (O) and finally polymers (P) was proposed to account for a clear lack of mass balance closure (Fig. 1). Similar to the previous work [32] oligomers were considered to originate from the reactant because of a lack of the mass balance closure already at the beginning of experiments, even if in general other substrates can lead to deactivation.

The equations for the reaction rates presented in Fig. 1 were written based on the approach of Langmuir-Hinshelwood with competitive adsorption of oxygen as illustrated below for the transformation of the reactant to betulinic aldehyde (reaction 1 in Fig. 1):

$$r_1 = \frac{k_1 K_A C_A}{(1 + K_A C_A + K_B C_B + K_C C_C + K_D C_D + K_{O_2} P_{O_2})} + \frac{k_{11} K_A C_A K_{O_2} P_{O_2}}{(1 + K_A C_A + K_B C_B + K_C C_C + K_D C_D + K_{O_2} P_{O_2})^2} \quad (2)$$

where C_A, etc. is the concentration in mol/L, K is the adsorption coefficient in L/mol and P_{O_2} is the pressure of oxygen in bar.

Two terms in Eq. (2) correspond to dehydrogenation of betulin in anaerobic conditions and oxidation in the presence of air respectively, thus giving different order in the denominator containing adsorption terms. Oxygen was considered to adsorb without dissociation. In the previous study [32] experiments were performed at one pressure of oxygen, thus dependence of the oxygen concentration was implicitly incorporated in the rate constants k_i.

Similar to Eq. (2) expressions for reactions 2–4 the rate expressions are essentially very much the same:

$$r_2 = \frac{k_2 K_A C_A}{(1 + K_A C_A + K_B C_B + K_C C_C + K_D C_D + K_{O_2} P_{O_2})} + \frac{k_{22} K_A C_A K_{O_2} P_{O_2}}{(1 + K_A C_A + K_B C_B + K_C C_C + K_D C_D + K_{O_2} P_{O_2})^2} \quad (3)$$

$$r_3 = \frac{k_3 K_C C_C}{(1 + K_A C_A + K_B C_B + K_C C_C + K_D C_D + K_{O_2} P_{O_2})} + \frac{k_{33} K_C C_C K_{O_2} P_{O_2}}{(1 + K_A C_A + K_B C_B + K_C C_C + K_D C_D + K_{O_2} P_{O_2})^2} \quad (4)$$

$$r_4 = \frac{k_4 K_B C_B}{(1 + K_A C_A + K_B C_B + K_C C_C + K_D C_D + K_{O_2} P_{O_2})} + \frac{k_{44} K_B C_B K_{O_2} P_{O_2}}{(1 + K_A C_A + K_B C_B + K_C C_C + K_D C_D + K_{O_2} P_{O_2})^2} \quad (5)$$

While less mechanistic information is available on oligomerization and polymerization, it is reasonable to assume that they are of the second order, while depolymerization is of the first one.

$$r_5 = \frac{k_5 K_A^2 C_A^2}{(1 + K_A C_A + K_B C_B + K_C C_C + K_D C_D + K_{O_2} P_{O_2})^2} \quad (6)$$

$$r_{-5} = \frac{k_{-5} K_{oligomers} C_{oligomers}}{1 + K_A C_A + K_B C_B + K_C C_C + K_D C_D + K_{O_2} P_{O_2}} \quad (7)$$

$$r_6 = \frac{k_6 K^2{}_{oligomers} C^2_{oligomers}}{(1 + K_A C_A + K_B C_B + K_C C_C + K_D C_D + K_{O_2} P_{O_2})^2} \quad (8)$$

As the main aim of the kinetic analysis was to illustrate applicability of the mechanistic approach avoiding overparametrization only experiments at one temperature (140 °C) were used in the modeling, also taking into account that only few experiments were conducted at other temperatures.

Deactivation of the catalyst, which was not considered in the previous kinetic analysis explicitly [32], in the current study was incorporated in the current work by assuming that the relative fraction of catalytically sites f decreasing with reaction time according to:

$$f = \frac{a_t}{a_0} = e^{-k_{deactivation} P_{O_2} t} \quad (9)$$

where a_o is the initial activity and a_t is activity at time t.

Preliminary data fitting was done by assuming adsorption of all reactants. The initial parameter estimation demonstrated, however, that even if the initial rate display a maximum vs the substrate concentration, adequate description of the whole concentrations curve can be achieved by considering only adsorption of oxygen.

The mass balance equations for the main reactants are

$$-\frac{dC_A}{dt} = f\rho(r_1 + r_2 + r_5 - r_{-5});\ \frac{dC_B}{dt} = f\rho(r_2 - r_4)\frac{dC_C}{dt} = f\rho(r_1 - r_3);\ \frac{dC_D}{dt} = f\rho(r_3 + r_4) \quad (10)$$

where ρ is the catalyst bulk density (the ratio of the catalyst mass to the liquid volume).

The concentration of the oligomers and the polymers is respectively

$$\frac{dC_0}{dt} = f\rho(r_5 - r_{-5} - r_6); \frac{dC_P}{dt} = f\rho r_6 \quad (11)$$

the parameter estimation was performed with the simplex and Levenberg-Marquardt methods solving the differential Eqs. (10) and

Table 5
Calculated rate constants.

Constant	Units	Value	Relative error,%
$\rho k_1 K_A$	min^{-1}	$1.6\ 10^{-3}$	48.4
$\rho k_{11} K_A$	min^{-1}	$9.9\ 10^{-3}$	59.9
$\rho k_2 K_A$	min^{-1}	$6.1\ 10^{-3}$	14.6
$\rho k_{22} K_A$	min^{-1}	0.04	18.2
$\rho k_3 K_C$	min^{-1}	$1.4\ 10^{-4}$	>100
$\rho k_{33} K_C$	min^{-1}	$2.1\ 10^{-3}$	>100
$\rho k_4 K_B$	min^{-1}	0.296	53.8
$\rho k_{44} K_B$	min^{-1}	5.56	55.3
ρk_5	L/mmol/min	$2\ 10^{-3}$	>100
ρk_{-5}	min^{-1}	0.314	>100
ρk_6	L/mmol/min	0.33	>100
$k_{deactivation}$	$min^{-1}\ bar^{-1}$	$9.4\ 10^{-3}$	15.9
K_{O2}	bar^{-1}	0.92	16.7

(11) with the backward difference method incorporated in the optimization software ModEst [74].

The objective function Q was defined as the sum of the squared differences between the experimental and calculated concentrations of all components. The values of kinetic parameters are given in Table 5, illustrating that beside the constants for oligomerization/polymerization only for the reaction 3 the constants are poorly defined, which is understandable as betulonic aldehyde can be generated from both betulinic aldehyde and betulone not allowing discrimination between these pathways from the available data. The results of the calculations (Fig. 5) along with the high value of the degree of explanation (99.45%) illustrate that the model describes the experimental data rather well, being also able to address catalyst deactivation, which was omitted in the previous study [32].

4. Conclusions

In the current work, which is a continuation of a previous study of the betulin liquid-phase oxidation with air over supported Ag NPs catalysts, the kinetic regularities and the reasons of catalyst deactivation were revealed, and an approach for the catalyst regeneration was proposed.

The complex character of betulin oxidation, namely a consecutive-parallel reaction network, was reflected by kinetic regularities.

Temperature, the initial betulin concentration, oxygen content in the reactant gas, and catalyst loading, had a significant impact on the initial reaction rate, betulin conversion, mass balance closure established through GC analysis, and, accordingly, on the yield of the main

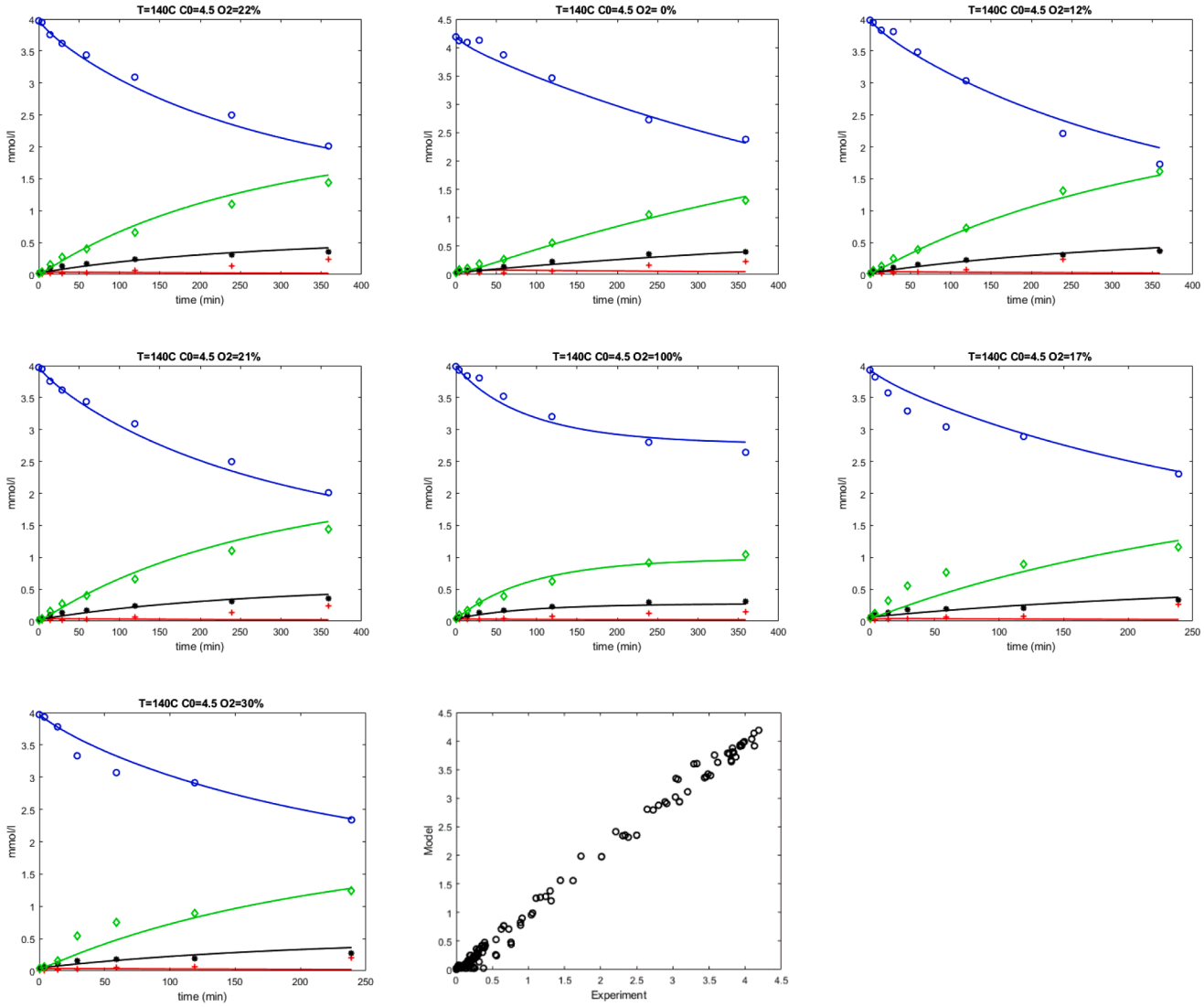

Fig. 5. Comparison between experimental (points) and calculated (lines) concentration profiles in betulin oxidation over Ag/Al catalyst. Conditions are given in the legend of each figure. Components A, B, C and D are color coded being blue, red, black and green respectively. The graph at the bottom left corresponds to the parity plot (experimental vs calculated concentration) for all data sets.

oxidation products (betulone, betulinic and betulonic aldehydes). In particular, betulin conversion was inversely dependent on its initial concentration, which is not typical for first-order reactions. At the same time, none of the varied experimental parameters affected the distribution of reaction products; the main product of betulin oxidation, in all cases, was betulonic aldehyde, followed by betulinic aldehyde and betulone. It was due to the activation energy required for the formation of these products. Betulonic aldehyde was formed as a result of betulone oxidation with the lowest activation energy.

Betulin oxidation with air over supported Ag NPs catalysts follows the Langmuir-Hinshelwood mechanism, which is clearly reflected in dependence of the initial reaction rate on the reagent concentrations (betulin and oxygen), displaying clear maxima.

An oxidizing environment and a relatively high temperature (140 °C) resulted in significant changes in the active surface of the catalyst. The equilibrium $Ag^0 \leftrightarrow Ag^+$ was shifted towards formation of silver oxide, while a higher mobility of the latter at 140 °C led during the catalytic process to an increase in the average size of silver NPs by almost 15 fold and a broader cluster size distribution. Similar changes were also revealed by varying the oxygen concentration in the reactant gas. Subsequently, aggregation of Ag NPs and a decrease in the fraction of metallic silver are one of the reasons for deactivation of nanosilver catalysts. Another reason was strong adsorption of the substrate/products on the catalyst surface as well as coking. The cumulative character of deactivation required a two-stage regeneration technique, namely, first in a mixture of 21% O_2 and 79% N_2 (air) at 500 °C for 3 h, followed by exposing to a mixture of 20% H_2 and 80% N_2 at 300 °C for 2 h.

Kinetic analysis was performed, illustrating that the Langmuir-Hinshelwood type of models considering competitive adsorption of oxygen and organic compounds as well as oxygen pressure dependent catalyst deactivation, can adequately describe experimental data.

Funding

The research is funded from Ministry of Education and Science of the Russian Federation Program No. 075–03–2021–287/6 (Russia).

CRediT authorship contribution statement

A. Grigoreva: Investigation, Writing – review & editing. **E. Kolobova:** Investigation, Writing – original draft, Writing – review & editing, Conceptualization, Methodology, Funding acquisition, Supervision. **E. Pakrieva:** Investigation, Writing – review & editing. **P. Mäki-Arvela:** Methodology, Writing – review & editing, Supervision. **S. Kuznetsova:** Investigation. **S.A.C. Carabineiro:** Investigation, Writing – review & editing, Supervision. **N. Bogdanchikova:** Supervision, Funding acquisition, Writing – review & editing. **A. Pestryakov:** Supervision, Funding acquisition, Writing – review & editing. **D.Yu. Murzin:** Conceptualization, Methodology, Supervision, Writing – review & editing.

Declaration of Competing Interest

The authors declare that they have no known competing financial interests or personal relationships that could have appeared to influence the work reported in this paper.

Acknowledgments

XPS measurements were carried out at the Central laboratories of Tomsk Polytechnic University (Analytical Center). HRTEM was carried out at the Innovation centre for Nanomaterials and Nanotechnologies of Tomsk Polytechnic University. The ICP-OES analysis was carried out using the core facilities of "Physics and Chemical methods of analysis" of Tomsk Polytechnic University. Fundação para a Ciência e a Tecnologia for Scientific Employment Stimulus Institutional Call (CEECINST/00102/2018), UIDB/50006/2020 and UIDP/50006/2020 (LAQV), UIDB/00100/2020 and UIDP/00100/2020 (Centro de Química Estrutural).

Supplementary materials

Supplementary material associated with this article can be found, in the online version, at doi:10.1016/j.mcat.2022.112461.

References

[1] F. Svoykin, A. Birman, I. Bacherikov, O. Mater, V. Bozhbov, Perspectives of bark dump recycling at wood processing enterprises, IOP Conf. Ser. Mater. Sci. Eng. 817 (2020), 012033, https://doi.org/10.1088/1757-899X/817/1/012033.
[2] E.W.H. Hayek, U. Jordis, W. Moche, F. Sauter, A bicentennial of betulin, Phytochemistry 28 (1989) 2229–2242, https://doi.org/10.1016/S0031-9422(00)97961-5.
[3] G.A. Tolstikov, O.B. Flekhter, E.E. Shultz, L.A. Baltina, A.G. Tolstikov, Betulin and its derivatives. Chemistry and biological activity, Chem. Sustain. Dev. 13 (2005) 1–29.
[4] R. Ekman, The suberin monomers and triterpenoids from the outer bark of Betula verrucosa Ehrh, Holzforschung 37 (1983) 205–211, https://doi.org/10.1515/hfsg.1983.37.4.205.
[5] S. Alakurtti, T. Mäkelä, S. Koskimies, J. Yli-Kauhaluoma, Pharmacological properties of the ubiquitous natural product betulin, Eur. J. Pharm. Sci. 29 (2006) 1–13, https://doi.org/10.1016/j.ejps.2006.04.006.
[6] S. Amiri, S. Dastghaib, M. Ahmadi, P. Mehrbod, F. Khadem, H. Behrouj, M. R. Aghanoori, F. Machaj, M. Ghamsari, J. Rosik, A. Hudecki, A. Afkhami, M. Hashemi, M.J. Los, P. Mokarram, T. Madrakian, S. Ghavami, Betulin and its derivatives as novel compounds with different pharmacological effects, Biotechnol. Adv. 38 (2020), 107409, https://doi.org/10.1016/j.biotechadv.2019.06.008.
[7] P.L. Sousa, R.O. da S. Souza, L.D. Tessarolo, R.R. de Menezes, T.L. Sampaio, J. A. Canuto, A.M.C. Martins, Betulinic acid induces cell death by necrosis in Trypanosoma cruzi, Acta Trop. 174 (2017) 72–75, https://doi.org/10.1016/j.actatropica.2017.07.003.
[8] Y. Wan, Y.L. Wu, L.H. Lian, W.X. Xie, X. Li, B.Q. Ouyang, T. Bai, Q. Li, N. Yang, J. X. Nan, The anti-fibrotic effect of betulinic acid is mediated through the inhibition of NF-κB nuclear protein translocation, Chem. Biol. Interact. 195 (2012) 215–223, https://doi.org/10.1016/j.cbi.2012.01.002.
[9] L. Pohjala, S. Alakurtti, T. Ahola, J. Yli-Kauhaluoma, P. Tammela, Betulin-derived compounds as inhibitors of alphavirus replication, J. Nat. Prod. 72 (2009) 1917–1926, https://doi.org/10.1021/np9003245.
[10] M. Liu, S. Yang, L. Jin, D. Hu, Z. Wu, S. Yang, Chemical constituents of the ethyl acetate extract of Belamcanda chinensis (L.) DC roots and their antitumor activities, Molecules 17 (2012) 6156–6169, https://doi.org/10.3390/molecules17056156.
[11] S. Alakurtti, P. Bergström, N. Sacerdoti-Sierra, C.L. Jaffe, J. Yli-Kauhaluoma, Anti-leishmanial activity of betulin derivatives, J. Antibiot. 63 (2010) 123–126, https://doi.org/10.1038/ja.2010.2 (Tokyo).
[12] C.P. Reyes, M.J. Núñez, I.A. Jiménez, J. Busserolles, M.J. Alcaraz, I.L. Bazzocchi, Activity of lupane triterpenoids from Maytenus species as inhibitors of nitric oxide and prostaglandin E_2, Bioorganic Med. Chem. 14 (2006) 1573–1579, https://doi.org/10.1016/j.bmc.2005.10.063.
[13] S. Haque, D.A. Nawrot, S. Alakurtti, L. Ghemtio, J. Yli-Kauhaluoma, P. Tammela, Screening and characterisation of antimicrobial properties of semisynthetic betulin derivatives, PLoS One 9 (2014), 102696, https://doi.org/10.1371/journal.pone.0102696.
[14] K. Hata, K. Hori, H. Ogasawara, S. Takahashi, Anti-leukemia activities of Lup-28-al-20(29)-en-3-one, a lupane triterpene, Toxicol. Lett. 143 (2003) 1–7, https://doi.org/10.1016/S0378-4274(03)00092-4.
[15] V. Zuco, R. Supino, S.C. Righetti, L. Cleris, E. Marchesi, C. Gambacorti-Passerini, F. Formelli, Selective cytotoxicity of betulinic acid on tumor cell lines, but not on normal cells, Cancer Lett. 175 (2002) 17–25, https://doi.org/10.1016/S0304-3835(01)00718-2.
[16] E. Bebenek, M. Kadela-Tomanek, E. Chrobak, M. Latocha, S. Boryczka, Novel triazoles of 3-acetylbetulin and betulone as anticancer agents, Med. Chem. Res. 27 (2018) 2051–2061, https://doi.org/10.1007/s00044-018-2213-x.
[17] R.C. Santos, J.A.R. Salvador, S. Marín, M. Cascante, Novel semisynthetic derivatives of betulin and betulinic acid with cytotoxic activity, Bioorganic Med. Chem. 17 (2009) 6241–6250, https://doi.org/10.1016/j.bmc.2009.07.050.
[18] K. Hata, K. Hori, S. Takahashi, Differentiation - and apoptosis-inducing activities by pentacyclic triterpenes on a mouse melanoma cell line, J. Nat. Prod. 65 (2002) 645–648, https://doi.org/10.1021/np0104673.
[19] X.K. Zhan, J.L. Li, S. Zhang, P.Y. Xing, M.F. Xia, Betulinic acid exerts potent antitumor effects on paclitaxel-resistant human lung carcinoma cells (H460) via G2/M phase cell cycle arrest and induction of mitochondrial apoptosis, Oncol. Lett. 16 (2018) 3628–3634, https://doi.org/10.3892/ol.2018.9097.
[20] P. Kumar, A.K. Singh, V. Raj, A. Rai, A.K. Keshari, D. Kumar, B. Maity, A. Prakash, S. Maiti, S. Saha, Poly(lactic-co-glycolic acid)-loaded nanoparticles of betulinic acid for improved treatment of hepatic cancer: characterization, *in vitro* and *in vivo* evaluations, Int. J. Nanomed. 13 (2018) 975–990, https://doi.org/10.2147/IJN.S157391.
[21] A.Q. Zeng, Y. Yan, Y.Q. Yao, F.F. Yang, M. Liao, L.J. Song, Y.L. Li, Y. Yu, L.Y. Jue, Y.L. Deng, S.P. Yang, C.J. Zeng, L. Ping, Y.M. Xie, J.L. Yang, Y.W. Zhang, T.H. Ye,

Y.Q. Wei, Betulinic acid impairs metastasis and reduces immunosuppressive cells in breast cancer models, Oncotarget 9 (2018) 3794–3804, https://doi.org/10.18632/oncotarget.23376.
[22] M.C. Lingaraju, N.N. Pathak, J. Begum, V. Balaganur, H.D. Ramachandra, R. A. Bhat, M. Ram, V. Singh, K. Kandasamy, D. Kumar, D. Kumar, S.K. Tandan, Betulinic acid attenuates renal oxidative stress and inflammation in experimental model of murine polymicrobial sepsis, Eur. J. Pharm. Sci. 70 (2015) 12–21, https://doi.org/10.1016/j.ejps.2015.01.001.
[23] J. Peng, Y.C. Lv, P.P. He, Y.Y. Tang, W. Xie, X.Y. Liu, Y. Li, G. Lan, M. Zhang, C. Zhang, J.F. Shi, X.L. Zheng, W.D. Yin, C.K. Tang, Betulinic acid downregulates expression of oxidative stress-induced lipoprotein lipase via the PKC/ERK/c-Fos pathway in RAW264.7 macrophages, Biochimie 119 (2015) 192–203, https://doi.org/10.1016/j.biochi.2015.10.020.
[24] M.A. Nader, H.N. Baraka, Effect of betulinic acid on neutrophil recruitment and inflammatory mediator expression in lipopolysaccharide-induced lung inflammation in rats, Eur. J. Pharm. Sci. 46 (2012) 106–113, https://doi.org/10.1016/j.ejps.2012.02.015.
[25] A. Halder, D. Shukla, S. Das, P. Roy, A. Mukherjee, B. Saha, Lactoferrin-modified betulinic acid-loaded PLGA nanoparticles are strong anti-leishmanials, Cytokine 110 (2018) 412–415, https://doi.org/10.1016/j.cyto.2018.05.010.
[26] A.N. Semenenko, N.L. Babak, A.M. Eremina, I.M. Gella, S.V. Shishkina, V. I. Musatov, V.V. Lipson, Chemical transformations of betulonic aldehyde, Russ. J. Org. Chem. 52 (2016) 249–260, https://doi.org/10.1134/S1070428016020160.
[27] K. Bowdenen, I.M. Heilbron, E.R.H. Jones, B.C.L. Weedon, Researches on acetylenic compounds. Part I .The preparation of acetylenic ketones by oxidation of acetylenic carbinols and glycols, J. Chem. Soc. (1946) 39–45.
[28] A. Barthel, S. Stark, R. Csuk, Oxidative transformations of betulinol, Tetrahedron 64 (2008) 9225–9229, https://doi.org/10.1016/j.tet.2008.07.042.
[29] A. Pichette, H. Liu, C. Roy, S. Tanguay, F. Simard, S. Lavoie, Selective oxidation of betulin for the preparation of betulinic acid, an antitumoral compound, Synth. Commun. 34 (2004) 3925–3937, https://doi.org/10.1081/SCC-200034788.
[30] R. Csuk, K. Schmuck, R. Schäfer, A practical synthesis of betulinic acid, Tetrahedron Lett. 47 (2006) 8769–8770, https://doi.org/10.1016/j.tetlet.2006.10.004.
[31] D.S.H.L. Kim, Z. Chen, T. van Nguyen, J.M. Pezzuto, S. Qiu, Z.Z. Lu, A concise semi-synthetic approach to betulinic acid from betulin, Synth. Commun. 27 (1997) 1607–1612, https://doi.org/10.1080/00397919708006099.
[32] E.N. Kolobova, E.G. Pakrieva, S.A.C. Carabineiro, N. Bogdanchikova, A. N. Kharlanov, S.O. Kazantsev, J. Hemming, P. Mäki-Arvela, A.N. Pestryakov, D. Y. Murzin, Oxidation of a wood extractive betulin to biologically active oxo-derivatives using supported gold catalysts, Green Chem. 21 (2019) 3370–3382, https://doi.org/10.1039/c9gc00949c.
[33] E. Kolobova, P. Mäki-Arvela, A. Grigoreva, E. Pakrieva, S.A.C. Carabineiro, J. Peltonen, S. Kazantsev, N. Bogdanchikova, A. Pestryakov, D.Y. Murzin, Catalytic oxidative transformation of betulin to its valuable oxo-derivatives over gold supported catalysts: effect of support nature, Catal. Today 367 (2021) 95–110, https://doi.org/10.1016/j.cattod.2020.07.051.
[34] E. Kolobova, Y. Kotolevich, E. Pakrieva, G. Mamontov, M.H. Farias, V. Cortés Corberán, N. Bogdanchikova, J. Hemming, A. Smeds, P. Mäki-Arvela, D.Y. Murzin, A. Pestryakov, Modified Ag/TiO_2 systems: promising catalysts for liquid-phase oxidation of alcohols, Fuel 234 (2018) 110–119, https://doi.org/10.1016/j.fuel.2018.06.128.
[35] N.D. Shcherban, P. Mäki-Arvela, A. Aho, S. Sergiienko, M.A. Skoryk, E. Kolobova, I. L. Simakova, K. Eränen, A. Smeds, J. Hemming, D.Y. Murzin, Preparation of betulone via betulin oxidation over Ru nanoparticles deposited on graphitic carbon nitride, Catal. Lett. 149 (2019) 723–732, https://doi.org/10.1007/s10562-018-02649-8.
[36] P. Mäki-Arvela, M. Barsukova, I. Winberg, A. Smeds, J. Hemming, K. Eränen, A. Torozova, A. Aho, K. Volcho, D.Y. Murzin, Unprecedented selective heterogeneously catalysed "green" oxidation of betulin to biologically active compounds using synthetic air and supported Ru catalysts, ChemistrySelect 1 (2016) 3866–3869, https://doi.org/10.1002/slct.201600731.
[37] A. Grigoreva, E. Kolobova, E. Pakrieva, P. Mäki-Arvela, S.A.C. Carabineiro, A. Gorbunova, N. Bogdanchikova, D. Murzin, A. Pestryakov, Supported silver nanoparticles as catalysts for liquid-phase betulin oxidation, Nanomaterials 11 (2021) 469, https://doi.org/10.3390/nano11020469.
[38] K.I. Shimizu, A. Satsuma, Silver cluster catalysts for green organic synthesis, J. Jpn. Pet. Inst. 54 (2011) 347–360, https://doi.org/10.1627/jpi.54.347.
[39] N. Kolobova, N. Pestryakov, N. Bogdanchikova, V. Cortés Corberán, Silver catalysts for liquid-phase oxidation of alcohols in green chemistry: challenges and outlook, Catal. Today 333 (2019) 81–88, https://doi.org/10.1016/j.cattod.2018.06.030.
[40] T. Chakraborty, A. Chakraborty, S. Maity, D. Das, T. Chattopadhyay, Conglomerated system of Ag nanoparticles decorated Al_2O_3 supported cobalt and copper complexes with enhanced catalytic activity for oxidation reactions, Mol. Catal 462 (2019) 104–113, https://doi.org/10.1016/j.mcat.2018.11.003.
[41] D. Zhao, T. Su, Y. Wang, R.S. Varma, C. Len, Recent advances in catalytic oxidation of 5-hydroxymethylfurfural, Mol. Catal. 495 (2020), 111133, https://doi.org/10.1016/j.mcat.2020.111133.
[42] V.V. Torbina, A.A. Vodyankin, S. Ten, G.V. Mamontov, M.A. Salaev, V.I. Sobolev, O.V. Vodyankina, Ag-based catalysts in heterogeneous selective oxidation of alcohols: a review, Catalysts 8 (2018) 447, https://doi.org/10.3390/catal8100447.
[43] M.J. Beier, T.W. Hansen, J.D. Grunwaldt, Selective liquid-phase oxidation of alcohols catalyzed by a silver-based catalyst promoted by the presence of ceria, J. Catal. 266 (2009) 320–330, https://doi.org/10.1016/j.jcat.2009.06.022.
[44] S.F. Adil, M.E. Assal, M. Khan, A. Al-Warthan, M.H. Rafiq Siddiqui, Nano silver-doped manganese oxide as catalyst for oxidation of benzyl alcohol and its derivatives: synthesis, characterisation, thermal study and evaluation of catalytic properties, Oxid. Commun. 36 (2013) 778–791.
[45] B. Zahed, H. Hosseini-Monfared, A comparative study of silver-graphene oxide nanocomposites as a recyclable catalyst for the aerobic oxidation of benzyl alcohol: support effect, Appl. Surf. Sci. 328 (2015) 536–547, https://doi.org/10.1016/j.apsusc.2014.12.078.
[46] J.F. Moulder, W.F. Stickle, P.E. Sobol, K.D. Bomben, J. Chastain, Handbook of X-ray Photoelectron Spectroscopy, Perkin-Elmer Corporation: Eden Prairie, MN, USA, 1992.
[47] D. Briggs, H. Adhes, D.E. Packham, X-ray Photoelectron Spectroscopy (XPS), 2nd ed., John Wiley & Sons, 2005, pp. 621–622, https://doi.org/10.1002/0470014229.ch22. Ed.
[48] F. Balikci, S.B. Yuceer, C. Guldur, Comparative study of Ag_2O/Co_3O_4 catalysts prepared by the sol-gel and co-precipitation Techniques: characterization and CO activity studies, Chem. Eng. Commun. 196 (2009) 171–181, https://doi.org/10.1080/00986440802290169.
[49] G.B. Hoflund, Z.F. Hazos, G.N. Salaita, Surface characterization study of Ag, AgO, and Ag_2O using x-ray photoelectron spectroscopy and electron energy-loss spectroscopy, Phys. Rev. B 62 (2000) 11126–11133, https://doi.org/10.1103/PhysRevB.62.11126.
[50] Y. Wang, Z. Qu, J. Xu, B. Huang, Effect of Al_2O_3 phase on the catalytic performance for HCHO oxidation over Ag/Al_2O_3 catalysts, Appl. Catal. A Gen. 602 (2020), 117705, https://doi.org/10.1016/j.apcata.2020.117705.
[51] S. Chang, M. Li, Q. Hua, L. Zhang, Y. Ma, B. Ye, W. Huang, Shape-dependent interplay between oxygen vacancies and Ag-CeO_2 interaction in Ag/CeO_2 catalysts and their influence on the catalytic activity, J. Catal. 293 (2012) 195–204, https://doi.org/10.1016/j.jcat.2012.06.025.
[52] M.I. Mejía, G. Restrepo, J.M. Marín, R. Sanjines, C. Pulgarín, E. Mielczarski, J. Mielczarski, J. Kiwi, Magnetron-sputtered Ag surfaces. New evidence for the nature of the Ag ions intervening in bacterial inactivation, ACS Appl. Mater. Interfaces 2 (2010) 230–235, https://doi.org/10.1021/am900662q.
[53] I. Lopez-Salido, D.C. Lim, Y.D. Kim, Ag nanoparticles on highly ordered pyrolytic graphite (HOPG) surfaces studied using STM and XPS, Surf. Sci. 588 (2005) 6–18, https://doi.org/10.1016/j.susc.2005.05.021.
[54] G. Kutluk, M. Nakatake, H. Sumida, H. Namatame, M. Taniguchi, Electronic structure of supported metal nanoparticles, Phys. Rev. B 27 (1983) 748–762, https://doi.org/10.1063/1.3463367.
[55] P. Mäki-Arvela, G. Martin, I. Simakova, A. Tokarev, J. Wärnå, J. Hemming, B. Holmbom, T. Salmi, D.Y. Murzin, Kinetics, catalyst deactivation and modeling in the hydrogenation of β-sitosterol to β-sitostanol over microporous and mesoporous carbon supported Pd catalysts, Chem. Eng. J. 154 (2009) 45–51, https://doi.org/10.1016/j.cej.2009.01.022.
[56] D.Y. Murzin, T. Salmi, Kinetics of catalytic reactions with multiple/multifunctional catalysts. Catalytic Kinetics: Chemistry and Engineering, 2nd ed., Elsevier, 2016, pp. 447–496, https://doi.org/10.1016/b978-0-444-63753-6.00008-7.
[57] O.A. Simakova, E.V. Murzina, A.R. Leino, P. Mäki-Arvela, S. Willför, D.Y. Murzin, Gold catalysts for selective aerobic oxidation of the lignan hydroxymatairesinol to oxomatairesinol: catalyst deactivation and regeneration, Catal. Lett. 142 (2012) 1011–1019, https://doi.org/10.1007/s10562-012-0855-8.
[58] R.A. Van Santen, H.P.C.E. Kuipers, The mechanism of ethylene epoxidation, Adv. Catal. 35 (1987) 265–321, https://doi.org/10.1016/s0360-0564(08)60095-4.
[59] Y.L. Sandler, D.D. Durigan, The desorption and isotopic exchange of oxygen at a silver surface, J. Phys. Chem. 69 (1965) 4201–4207.
[60] P.A. Kilty, N.C. Rol, W.M.H. Sachtler, Identification of oxygen complexes adsorbed on silver and their function in the catalytic oxidation of ethylene, in: J. W. Hightower (Ed.), Proceedings, 5th Int. Congr, North Holland Publishing Company, Amsterdam, 1973, p. 929.
[61] A. Nagy, G. Mestl, High temperature partial oxidation reactions over silver catalysts, Appl. Catal. A Gen. 188 (1999) 337–353, https://doi.org/10.1016/S0926-860X(99)00246-X.
[62] V.M. Gryaznov, S.G. Gulyanova, S.G. Canisius, Investigation of oxygen diffusion through a silver membrane, J. Phys. Chem. 47 (1973) 2694–2699.
[63] V.I. Bukhtiyarov, Modern trends in the development of surface science as applied to catalysis. Establishment of the relationship between structure and activity for heterogeneous catalysts, Adv. Chem. 76 (2007) 596–627.
[64] M. Deng, G. Zhao, Q. Xue, L. Chen, Y. Lu, Microfibrous-structured silver catalyst for low-temperature gas-phase selective oxidation of benzyl alcohol, Appl. Catal. B Environ. 99 (2010) 222–228, https://doi.org/10.1016/j.apcatb.2010.06.023.
[65] J. Shen, W. Shan, Y. Zhang, J. Du, H. Xu, K. Fan, W. Shen, Y. Tang, Gas-phase selective oxidation of alcohols: *in situ* electrolytic nano-silver/zeolite film/copper grid catalyst, J. Catal. 237 (2006) 94–101, https://doi.org/10.1016/j.jcat.2005.10.027.
[66] F. Gunnarsson, H. Kannisto, M. Skoglundh, H. Härelind, Improved low-temperature activity of silver-alumina for lean NO_x reduction - effects of Ag loading and low-level Pt doping, Appl. Catal. B Environ. 152–153 (2014) 218–225, https://doi.org/10.1016/j.apcatb.2014.01.043.
[67] R. Bartolomeu, B. Azambre, A. Westermann, A. Fernandes, R. Bértolo, H. I. Hamoud, C. Henriques, P. Da Costa, F. Ribeiro, Investigation of the nature of silver species on different Ag-containing NO_x reduction catalysts: on the effect of the support, Appl. Catal. B Environ. 150–151 (2014) 204–217, https://doi.org/10.1016/j.apcatb.2013.12.021.
[68] R. Bartolomeu, R. Bértolo, S. Casale, A. Fernandes, C. Henriques, P. Da Costa, F. Ribeiro, Particular characteristics of silver species on Ag-exchanged LTL zeolite in K and H form, Microporous Mesoporous Mater. 169 (2013) 137–147, https://doi.org/10.1016/j.micromeso.2012.10.015.

[69] S. Fogel, D.E. Doronkin, P. Gabrielsson, S. Dahl, Optimisation of Ag loading and alumina characteristics to give sulphur-tolerant Ag/Al_2O_3 catalyst for H_2-assisted NH_3-SCR of N_x, Appl. Catal. B Environ. 125 (2012) 457–464, https://doi.org/10.1016/j.apcatb.2012.06.014.
[70] A. Flura, F. Can, X. Courtois, S. Royer, D. Duprez, High-surface-area zinc aluminate supported silver catalysts for low-temperature SCR of NO with ethanol, Appl. Catal. B Environ. 126 (2012) 275–289, https://doi.org/10.1016/j.apcatb.2012.07.006.
[71] A.N. Pestryakov, A.A. Davydov, Study of supported silver states by the method of electron spectroscopy of diffuse reflectance, J. Electron Spectros. Relat. Phenom. 74 (1995) 195–199, https://doi.org/10.1016/0368-2048(95)02371-2.
[72] M.D. Argyle, C.H. Bartholomew, Heterogeneous catalyst deactivation and regeneration: a review, Catalysts 5 (2015) 145–269, https://doi.org/10.3390/catal5010145.
[73] A.V. Bukhtiyarov, A.Y. Stakheev, A.I. Mytareva, I.P. Prosvirin, V.I. Bukhtiyarov, *In situ* XPS study of the size effect in the interaction of NO with the surface of the model Ag/Al_2O_3/FeCrAl catalysts, Russ. Chem. Bull. 64 (2015) 2780–2785, https://doi.org/10.1007/s11172-015-1225-7.
[74] H. Haario, ModEst, Modelling and Optimization Software, Profmath Oy, Helsinki, 2001.